

Spatial Range of Autocrine Signaling: Modeling and Computational Analysis

Stanislav Y. Shvartsman,* H. Steven Wiley,[§] William M. Deen,*[†] and Douglas A. Lauffenburger*^{†‡}

*Department of Chemical Engineering, [†]Division of Bioengineering and Environmental Health, [‡]Center for Cancer Research, Massachusetts Institute of Technology, Cambridge, Massachusetts 02139, and [§]Environmental and Health Sciences Division, Pacific Northwest National Laboratory, Richland, Washington 99352 USA

ABSTRACT Autocrine loops formed by growth factors and their receptors have been identified in a large number of developmental, physiological, and pathological contexts. In general, the spatially distributed and recursive nature of autocrine signaling systems makes their experimental analysis, and often even their detection, very difficult. Here, we combine Brownian motion theory, Monte Carlo simulations, and reaction-diffusion models to analyze the spatial operation of autocrine loops. Within this modeling framework, the ability of autocrine cells to recapture the endogenous ligand and the distances traveled by autocrine ligands are explicitly related to ligand diffusion coefficients, density of surface receptors, ligand secretion rate, and rate constants of ligand binding and endocytic internalization. Applying our models to study autocrine loops in the epidermal growth factor receptor system, we find that autocrine loops can be highly localized—even at the level of a single cell. We demonstrate how the variations in molecular and cellular parameters may “tune” the spatial range of autocrine signals over several orders of magnitude: from microns to millimeters. We argue that this versatile regulation of the spatial range of autocrine signaling enables autocrine cells to perceive a broad spectrum of environmental information.

INTRODUCTION

Cells actively modify their environment (Werb and Yan, 1998). Membrane proteases degrade the extracellular matrix; receptors and proteoglycans shed from the cell surface selectively block the incoming signals; cells secrete soluble ligands that bind to receptors on their own surfaces. The last process defines an autocrine loop: a mode of cell signaling in which a cell both releases a soluble factor and responds to it (Sporn and Todaro, 1980; Sporn and Roberts, 1992). Autocrine loops formed by growth factors and their receptors are ubiquitous in cell biology and have been identified in a large number of normal and pathological contexts. At the same time, the principles governing their operation and their role in cell and tissue regulation are largely unexplored. A distinguishing characteristic of autocrine systems is their structural complexity, stemming both from the multiplicity of their components and from the variety of mechanisms through which these components can be regulated. Endogenous ligands are produced in extremely low amounts and are suspected to operate at submicron dimensions. These factors make the experimental analysis, and even the detection, of autocrine loops exceedingly difficult (Lauffenburger et al., 1998; DeWitt et al., 2001).

Over the past few years, much has been learned about important characteristics of autocrine loops from the studies of

engineered epidermal growth factor receptor (EGFR) systems (Dong, 1999; Shi et al., 2000; Lauffenburger et al., 1998; DeWitt et al., 2001; Oehrtman et al., 1998; Lauffenburger et al., 1995). In particular, it has been found that autocrine cells can be extremely efficient in processing and responding to secreted ligands, and that autocrine loops appear to function in a spatially localized manner (Lauffenburger et al., 1998; Dong et al., 1999). For example, EGFR ligands made at the basolateral surface of polarized epithelial cells do not enter the bulk medium unless the EGFR are blocked (Kuwada et al., 1998). Similar observations have been made in related contexts: e.g., regulatory cascades stimulated by the spatially restricted networks of paracrine and autocrine growth factors were identified at various stages of *Drosophila* development (Casici and Freeman, 1999), in bone remodeling (Goldring and Goldring, 1996), and in wound healing (Tokumaru et al., 2000). Although the mechanism of self-stimulation involving the autocrine release of growth factors and cytokines appears to be universal, little is known about the length scale over which any given autocrine loop operates, or about the molecular and cellular properties that govern the spatial range of autocrine signals.

A mechanistic model relating the operation of autocrine loops to their structural components can assist their experimental detection and guide the development of strategies for their manipulation. The need to manipulate autocrine loops arises both in bioengineering and in medicine. For example, autocrine loops can be harnessed to achieve cell proliferation under serum-free conditions; at the same time, autocrine loops are frequently used as a target in anti-cancer therapies. Here, we have combined theory and computations to provide a spatially resolved description of autocrine loops. To illustrate, we have used our models to analyze autocrine loops in the EGFR system.

Received for publication 21 September 2000 and in final form 29 June 2001.

Address reprint requests to Douglas A. Lauffenburger, MIT, Dept. of Chemical Engineering, Bldg. 56, Room 341, Cambridge, MA 02139. Tel.: 617-252-1629; Fax: 617-258-0204; E-mail: lauffen@mit.edu.

Dr. Shvartsman's current address is Dept. of Chemical Engineering and Lewis Sigler Institute for Integrative Genomics, Princeton University, Princeton, NJ 08540.

The paper is organized as follows: In the next section, we describe a continuum reaction-diffusion model for a single autocrine cell. We state the governing equations and determine the key dimensionless groups characterizing cell's ability to recapture the endogenous ligand. Following that, we use Brownian motion theory and stochastic simulations to characterize random paths followed by autocrine ligands. Our results explicitly relate the spatiotemporal properties of these paths to ligand diffusion constants, density of surface receptors, and rate constants of ligand binding and endocytic internalization. Finally, we use both approaches to examine autocrine loops in the EGFR system. In the final section, we discuss the recently proposed "cell sonar" hypothesis (Lauffenburger et al., 1998), according to which cells use the spatially restricted networks of autocrine growth factors to actively probe their microenvironment.

CONTINUUM MODEL OF BINDING AND TRANSPORT

In this section, we use a continuum reaction-diffusion model to analyze transport and binding in an autocrine system. We consider a single autocrine cell. Our analysis enables the computation of the fraction of endogenous ligand recaptured by the autocrine cell, and the evaluation of the transient ligand-receptor binding in an autocrine cell. First, we analyze the transient problem, deriving the reduced binding/transport model that depends only on the concentration of surface receptors and ligand/receptor complexes. Our continuum model is similar to the one followed by Shoup and Szabo (1982); Goldstein and Dembo (1995); Berg and Purcell (1977); and Starbuck et al. (1990). A hybrid stochastic/deterministic approach to modeling of autocrine loops has been proposed by (Forsten and Lauffenburger, 1994b); our analysis is fully deterministic. Then, we solve the steady problem, deriving the equation for the steady probability of ligand recapture as a function of the measurable parameters of autocrine loops.

The model (Fig. 1 A) accounts for the concentration of endogenous ligand, L (moles/cm³), and the surface densities of free and occupied surface receptors: R_s (moles/cm²) and C_s (moles/cm²), respectively. The cell is modeled as a hemisphere with radius r_{cell} , placed on an infinite plane. This mimics an autocrine cell attached to a substrate; by symmetry arguments, the same model applies to binding and transport around an autocrine cell suspended in solution. We consider the axially symmetric spatial distribution of ligand around the cell. Ligand secretion is uniformly distributed over the cell surface, resulting in the steady flux of autocrine ligands, q (moles/s/cm²). Ligand released in the extracellular medium diffuses with constant D (cm²/s) and reversibly binds to cell surface receptors with the binding constant K_d (moles/cm³). The newly synthesized receptors arrive to the cell surface with the flux s (moles/s/cm²); they are constitutively internalized with the rate constant k_c

(s⁻¹), and are converted to surface complexes with the rate constant k_{on} (moles⁻¹ cm³ s⁻¹). Surface complexes dissociate with the rate constant $k_{\text{off}} = k_{\text{on}}K_d$ (s⁻¹) and are endocytosed with rate constant k_e (s⁻¹).

The governing equations and boundary conditions are

$$\frac{\partial L}{\partial t} = D \left[\frac{\partial^2 L}{\partial r^2} + \frac{2}{r} \frac{\partial L}{\partial r} \right], \quad (1)$$

$$\frac{dR_s}{dt} = -k_{\text{on}}R_sL(r_{\text{cell}}) + k_{\text{off}}C + s - k_cR_s, \quad (2)$$

$$\frac{dC}{dt} = k_{\text{on}}R_sL - k_{\text{off}}C - k_eC, \quad (3)$$

$$D \frac{\partial L(r_{\text{cell}}, t)}{\partial r} = -q + k_{\text{on}}R_sL - k_{\text{off}}C, \quad L(\infty, t) = 0. \quad (4)$$

The system of equations is rendered dimensionless by the transformations,

$$\rho = \frac{r}{r_{\text{cell}}}, \quad \tau = k_{\text{off}}t, \quad \bar{L} = \frac{L}{K_d}, \quad (5)$$

$$\bar{C} = \frac{C_s}{s/k_c}, \quad \bar{R} = \frac{R_s}{s/k_c}.$$

The coordinate is scaled by the cell radius; the time is scaled by the inverse dissociation rate constant; ligand concentration is scaled by the equilibrium binding constant; the surface densities of free and occupied receptors are scaled by the density of receptors in the absence of ligand ($R_T \equiv s/k_c$). The rescaled problem becomes

$$\varepsilon \frac{\partial \bar{L}}{\partial \tau} = \frac{\partial^2 \bar{L}}{\partial \rho^2} + \frac{2}{\rho} \frac{\partial \bar{L}}{\partial \rho}, \quad (6)$$

$$\frac{d\bar{R}}{d\tau} = -\bar{R}\bar{L}(1) + \gamma(1 - \bar{R}) + \bar{C}, \quad (7)$$

$$\frac{d\bar{C}}{d\tau} = \bar{R}\bar{L} - \frac{1}{1 - \delta} \bar{C}, \quad (8)$$

$$\frac{\partial \bar{L}(1, \tau)}{\partial \rho} = -Au + \delta Da \bar{R}\bar{L}, \quad \bar{L}(\infty, \tau) = 0. \quad (9)$$

Five dimensionless groups appear in Eqs. 6–9,

$$Au = \frac{qr_{\text{cell}}}{DK_d}, \quad Da = \frac{k_{\text{on}}r_{\text{cell}}s}{k_cD}, \quad \gamma = \frac{k_c}{k_{\text{off}}}, \quad (10)$$

$$\delta = \frac{k_e}{k_e + k_{\text{off}}}, \quad \varepsilon = \frac{r_{\text{cell}}^2 k_{\text{off}}}{D}.$$

The first of these dimensionless groups, Au , is the Autocrine number, the ratio of the ligand concentration at the cell

surface in the absence of surface receptors to the dissociation constant of a ligand-receptor pair. The second, Da , is recognized as the Damköhler number that quantifies the relative importance of ligand binding and transport (Deen, 1998). The third group, γ , compares the rates, with which free receptors are removed by constitutive internalization, to the rate with which they are freed by dissociating complexes. For a bound ligand, the fourth group, δ , defines the probability of being internalized. Finally, ε is the time scale for the extracellular diffusion.

The system of Eqs. 6–9 is nonlinear; its solution, in general, requires numerical methods. We have discretized the partial differential equation in this problem using equidistant finite differences. The semi-infinite domain was approximated by a large finite domain with the Dirichlet boundary condition at the outer boundary ($\bar{L}(r_{\text{outer}}) = 0$); the domain size of ten times the size the cell radius ($r_{\text{outer}} = 10$) provides an excellent approximation to the semi-infinite problem. Discretization leads to a large dynamical system for the evolution of the concentrations of ligand on the grid points and the surface densities of surface receptors and complexes. This system was solved using a fully implicit time-integration method with a sparse linear system solver. Numerical solution was used to check the accuracy of the simplified transport/binding model that can be derived from Eqs. 6–9.

For high values of the secreted growth factor diffusivity, concentrations of soluble species evolve on the time scale that is much shorter than that of surface receptors and ligand/receptor complexes. In this regime the binding/transport model can be simplified. Using a steady-state approximation for the concentration of endogenous ligand, we can solve for the value of this concentration at the surface of our autocrine cell,

$$\bar{L}(1) = \frac{Au + Da\bar{C}}{1 + Da\bar{R}}. \quad (11)$$

Substituting this expression into the dynamical balance for surface receptors and ligand/receptor complexes, we obtain the lumped model for binding and transport,

$$\frac{d\bar{R}}{d\tau} = -\bar{R} \frac{Au + Da\bar{C}}{1 + Da\bar{R}} + \gamma(1 - \bar{R}) + \bar{C}, \quad (12)$$

$$\frac{d\bar{C}}{d\tau} = \bar{R} \frac{Au + Da\bar{C}}{1 + Da\bar{R}} - \frac{\bar{C}}{1 - \delta}. \quad (13)$$

By construction, the steady state of the lumped system is identical to that of the full model (Eqs. 6–9). Furthermore, for small values of parameter ε dynamics of the lumped model is in excellent agreement with that of the full model, Eqs. 6–9.

We can now analyze the steady probability for ligand recapture. Defining f to be the steady mass flux of ligand from the cell surface: $f = D(\partial L(r_{\text{cell}})/\partial r)$, the fraction of

endogenous ligand that escapes from the autocrine cell is found as f/q . The remaining fraction of the secreted ligand defines the (steady) probability of ligand capture, $P_{\text{cap}} = 1 - f/q$. Finding the steady state of Eqs. 7–8 as a function of ligand concentration at the cell surface, and then substituting this expression into the analytical solution of the boundary value problem for the extracellular ligand (Eqs. 6 and 9), P_{cap} is expressed as a function of Au , Da , γ , and δ ,

$$Da = \frac{P_{\text{cap}}Au}{\gamma} + \frac{P_{\text{cap}}}{\delta(1 - P_{\text{cap}})}. \quad (14)$$

The classic Berg/Purcell expression, $P_{\text{cap}} = Da/(1 + Da)$ (Berg and Purcell, 1977), is recovered in the limits of infinitely fast ligand internalization or negligible rate constant of complex dissociation. At $Au = 0$, P_{cap} simplifies to $P_{\text{cap}} = Da\delta/(1 + Da\delta)$. At low autocrine numbers, i.e., low secretion rates, we can use the implicit function theorem to approximate P_{cap} as

$$P_{\text{cap}} \approx \frac{Da\delta}{1 + Da\delta} - \frac{Au\delta}{\gamma(1 + Da\delta)^2}. \quad (15)$$

This captures the initial decrease in the fraction of recaptured ligand with the increase in the ligand secretion rate. When transport is rate limiting ($Da\delta \gg 1$), the last expression becomes $P_{\text{cap}} \approx 1 - Au/\delta\gamma Da^2$.

ANALYSIS OF LIGAND TRAJECTORIES

In this section, we use Brownian motion theory and stochastic simulations to analyze the statistical properties of random paths followed by autocrine ligands from the point of their release on the cell surface until their removal from the extracellular medium (Fig. 1 B). Our results are in the form of cumulative probability distribution functions that relate the spatiotemporal properties of random trajectories to the measurable parameters of autocrine systems. In particular, we focus on the spatial and temporal extrema of the trajectories followed by autocrine ligands. This leads to the estimates of the spatial and temporal ranges of autocrine loops.

Our analysis is based on a model in which a ligand is represented by a point particle that is released at the origin and randomly moves in the half-space above the plane covered by reversible traps that represent surface receptors (Wang et al., 1992; Lagerholm and Thompson, 1998; Forsten and Lauffenburger, 1994a; Agmon and Edelstein, 1997). Transport of autocrine ligands in the extracellular space is modeled as the three-dimensional Brownian motion. The distribution of surface receptors is assumed to be uniform in space and time. Surface complexes, produced when a ligand binds to one of the surface receptors, diffuse in two dimensions and are removed from the surface by internalization and dissociation. The dissociated ligand, again, moves in the half-space above the plane covered by

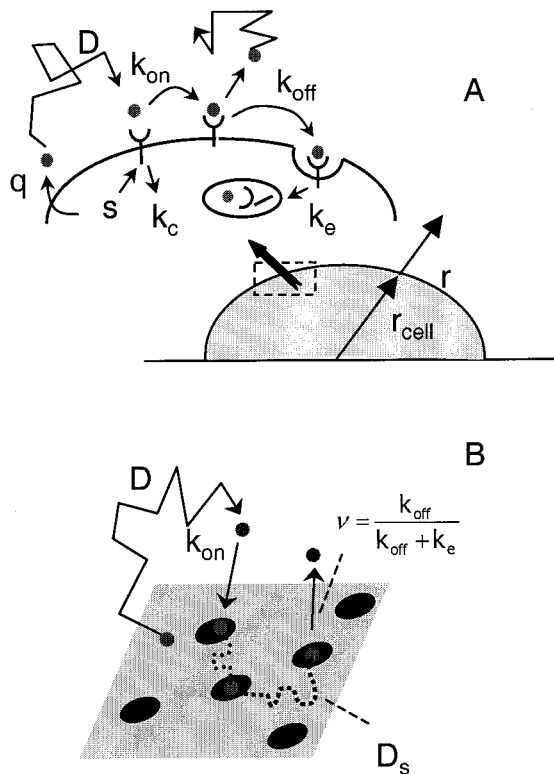


FIGURE 1 Models of binding and transport in autocrine systems. (A) Continuum model. A cell is modeled as a hemisphere with radius r_{cell} placed on a plane that does not absorb secreted ligand. The model accounts for the surface densities of receptors and ligand-receptor complexes, and for the radial distribution of endogenous ligand. The inset shows the main physical processes: receptor synthesis and constitutive degradation, ligand secretion at constant rate, diffusion, reversible binding, and endocytosis. (B) Stochastic model. A Brownian particle is released at the surface randomly covered by reversible traps. Each trajectory is composed of a random number of two- and three-dimensional “segments.” Bound particle is removed from the surface by a combination of two first-order processes: in one of these processes, the particle is again released into the half-space above the plane, the other process terminates the trajectory.

receptors plane until the next binding event. Thus, a trajectory followed by a ligand from the time of its release until its internalization is composed of an equal number of two- and three-dimensional random “segments” (see Fig. 2 A). Four random numbers can be associated with each composite trajectory: Z_{max} and R_{max} denote the maximal excursions in space, T_{max} is the time interval between the particle’s release and internalization, and $2N$ is the number of segments. The cumulative distribution functions $P\{Z_{\text{max}} \leq z\}$, $P\{R_{\text{max}} \leq r\}$, and $P\{T_{\text{max}} \leq t\}$ quantify the spatiotemporal extent of autocrine loops. By containing the information about the statistical properties of the extremal properties of ligand trajectories, these distributions provide quantitative estimates in answering the following question: how far do autocrine signaling loops extend into the cell’s microenvironment? For example, the probability $P\{Z_{\text{max}} \leq z\}$ characterizes the maximal distance traveled by the secreted ligand normal to the cell surface.

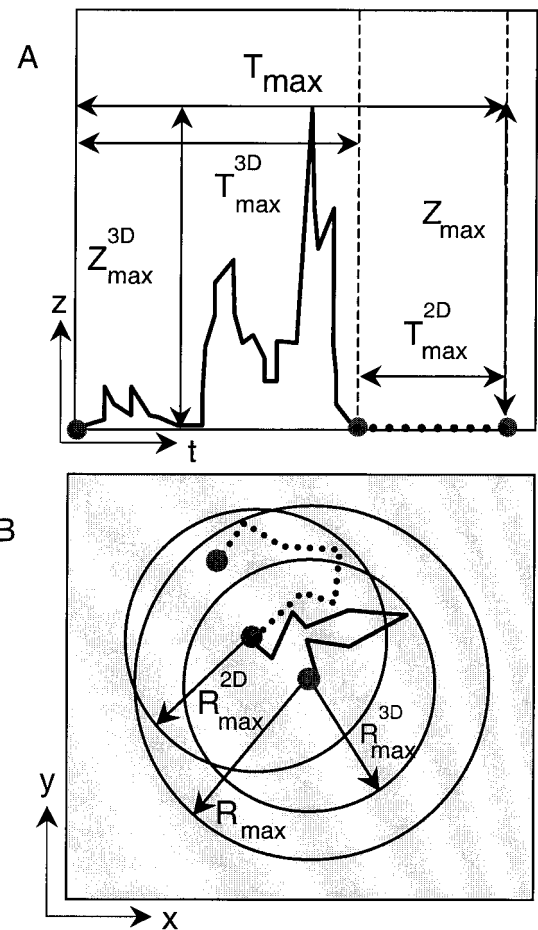


FIGURE 2 Definition of the random variables that characterize stochastic trajectories (see text for details). Every trajectory is composed of an equal number of two- and three-dimensional segments. Random variables characterizing the composite trajectories are related to the corresponding random numbers of the individual segments. In this example, the ligand is internalized after the first binding event and the composite trajectory consists of one three-dimensional and one two-dimensional segment. Maximal radial displacement of the composite trajectory, R_{max} , is bounded from above by $\bar{R}_{\text{max}} = R_{\text{max}}^{2\text{D}} + R_{\text{max}}^{3\text{D}}$, the sum of maximal displacements in two and three dimensions. In (B). The solid and dashed lines represent the radial parts of the two- and three-dimensional segments, respectively. Trajectory is terminated after $T_{\text{max}} = T_{\text{max}}^{3\text{D}} + T_{\text{max}}^{2\text{D}}$. Maximal vertical displacement is $Z_{\text{max}}^{3\text{D}}$, (A).

In the model, we do not restrict the motion of Brownian particles, allowing for arbitrarily large lateral and vertical displacements prior to capture. Although, in reality, the finite size of the cell and system boundaries influence the transport of autocrine ligands, analysis of ligand motion in an unbounded case is quite useful. As far as lateral constraints on the trajectory are concerned, our analysis is applicable to the analysis of transport above a confluent monolayer or an epithelial layer of autocrine cells. See Freeman (2000) for many examples of this problem in the context of developmental biology. In addition, the rates with which the spatial distribution functions approach unity, as

their arguments increase, indicate whether secreted ligands are captured before they reach an absorbing boundary placed at the argument of the distribution function. For example, the probability $P\{Z_{\max} \leq z\}$ can be interpreted as the probability of the particle being absorbed before reaching the perfectly absorbing boundary located at the height z above the layer of autocrine cells.

The number of segments in a composite trajectory is related to the probability of ligand internalization. From the previous section, this probability is given by $\delta = k_e/(k_{\text{off}} + k_e)$. The number of “visits” to the surface, therefore, is a geometric random variable with parameter δ (Ross, 1972); hence, on the average, composite trajectories have $N = 1/\delta$ two-dimensional (and an equal number of three-dimensional) segments.

Consider a particular composite trajectory consisting of $2N$ segments as in Fig. 2 *A* and *B*. Three random numbers are assigned to each of the N three-dimensional segments: $Z_{\max,i}^{3D}$ and $R_{\max,i}^{3D}$ denote the maximal vertical and lateral excursions of a particle, whereas $T_{\max,i}^{3D}$ is the time elapsed from the release of the ligand and to its next capture. In complete analogy, two random numbers can be associated with each of the N two-dimensional segments: $T_{\max,i}^{2D}$ is the duration of the i th visit to the surface, and $R_{\max,i}^{2D}$ is the maximal distance the particle diffuses before it is either internalized or dissociated. Random variables characterizing a composite trajectory are related to the corresponding random variables of the individual segments,

$$T_{\max} = \sum_{i=1}^N T_{\max,i}^{3D} + \sum_{i=1}^N T_{\max,i}^{2D} \quad (16)$$

$$Z_{\max} = \max\{Z_{\max,i}^{3D}\}_{i=1}^N \quad (17)$$

$$R_{\max} \leq \bar{R}_{\max} \equiv \sum_{i=1}^N R_{\max,i}^{3D} + \sum_{i=1}^N R_{\max,i}^{2D} \quad (18)$$

The last inequality follows from the fact that every trajectory can be fully enclosed by a cylinder with the radius \bar{R}_{\max} , equal to the sum of the maximal radial displacements of all the segments (Fig. 2 *B*). Hence, the cumulative distribution function of random variable \bar{R}_{\max} provides an upper bound for the lateral extent of autocrine loops,

$$P\{\bar{R}_{\max} \leq r\} \leq P\{R_{\max} \leq r\}. \quad (19)$$

At the end of this section, we describe efficient Monte Carlo algorithms for the numerical generation of the cumulative distribution functions of Z_{\max} , \bar{R}_{\max} , and T_{\max} . Our algorithms are based on direct generation of the random numbers Z_{\max}^{3D} , R_{\max}^{3D} , T_{\max}^{3D} , R_{\max}^{2D} , and T_{\max}^{2D} . The algorithms are direct in the sense that extremal properties of Brownian paths are obtained without simulation of the paths themselves. In Appendices A and B we illustrate how cumulative distribution functions for these random variables are de-

vised; here, we only summarize our analytical results. Note that the distribution of Z_{\max} , \bar{R}_{\max} , and T_{\max} are not independent of each other; they are distributed according to the joint multivariable distribution function. Here we report the marginal probability distributions for Z_{\max} , \bar{R}_{\max} , and T_{\max} . The joint distributions for the random variables characterizing the individual segments can be easily obtained from the linear boundary value problems stated in Appendices A and B.

The statistical properties of the three-dimensional segments depend on receptor density σ , forward ligand/receptor binding constant k_{on} , and the ligand diffusivity in the extracellular medium, D . In this approach, the receptor density, σ , can be identified with the surface density of unoccupied receptors in the continuum model (R_s). The cumulative distribution functions of the random variables T_{\max}^{3D} , R_{\max}^{3D} , and Z_{\max}^{3D} can be approximated by the following expressions (Appendix A):

$$P\{T_{\max}^{3D} \leq t\} \approx G_T \left(\sigma k_{\text{on}} \sqrt{\frac{t}{D}} \right) \equiv 1 - \text{Erfcx} \left(\sigma k_{\text{on}} \sqrt{\frac{t}{D}} \right), \quad (20)$$

$$P\{Z_{\max}^{3D} \leq z\} \approx G_Z \left(\frac{\sigma k_{\text{on}} z}{D} \right) \equiv \frac{\sigma k_{\text{on}} z / D}{1 + \sigma k_{\text{on}} z / D}, \quad (21)$$

$$P\{R_{\max}^{3D} \leq r\} \approx G_R \left(\frac{\sigma k_{\text{on}} r}{D} \right) > \frac{\sigma k_{\text{on}} r / D}{1.87 + \sigma k_{\text{on}} r / D}. \quad (22)$$

where Erfcx is the scaled complementary error function (Abramowitz and Stegun, 1964).

The statistical properties of the two-dimensional segments depend on the rate constants of dissociation, k_{off} , and endocytic internalization k_e , as well as on the diffusion coefficient of the bound ligand, D_s . In Appendix B, we derive the following expressions for the cumulative distribution functions of the random variables R_{\max}^{2D} and T_{\max}^{2D} :

$$P\{R_{\max}^{2D} \leq r\} = 1 - 1/I_0(r \sqrt{(k_e + k_{\text{off}})/D_s}), \quad (23)$$

$$P\{T_{\max}^{2D} \leq t\} = 1 - \exp[-(k_e + k_{\text{off}})t], \quad (24)$$

where I_0 is the modified Bessel function of the first kind of order zero (Abramowitz and Stegun, 1964).

In Fig. 3, each of the derived distributions is plotted as a function of the corresponding dimensionless variable. The cumulative distributions for R_{\max}^{3D} , Z_{\max}^{3D} , and T_{\max}^{2D} are easily invertible; hence, generation of the corresponding random variables is trivial. Generation of R_{\max}^{2D} and T_{\max}^{3D} is easily accomplished by numerical inversion. To generate each of the random variables, we generate a uniformly distributed random number and use it as an argument of the inverse of the cumulative distribution function (Dagpunar, 1988).

The foregoing provides a basis for the straightforward Monte Carlo algorithms for the generation of the random variables Z_{\max} , \bar{R}_{\max} , and T_{\max} . Each algorithm starts by

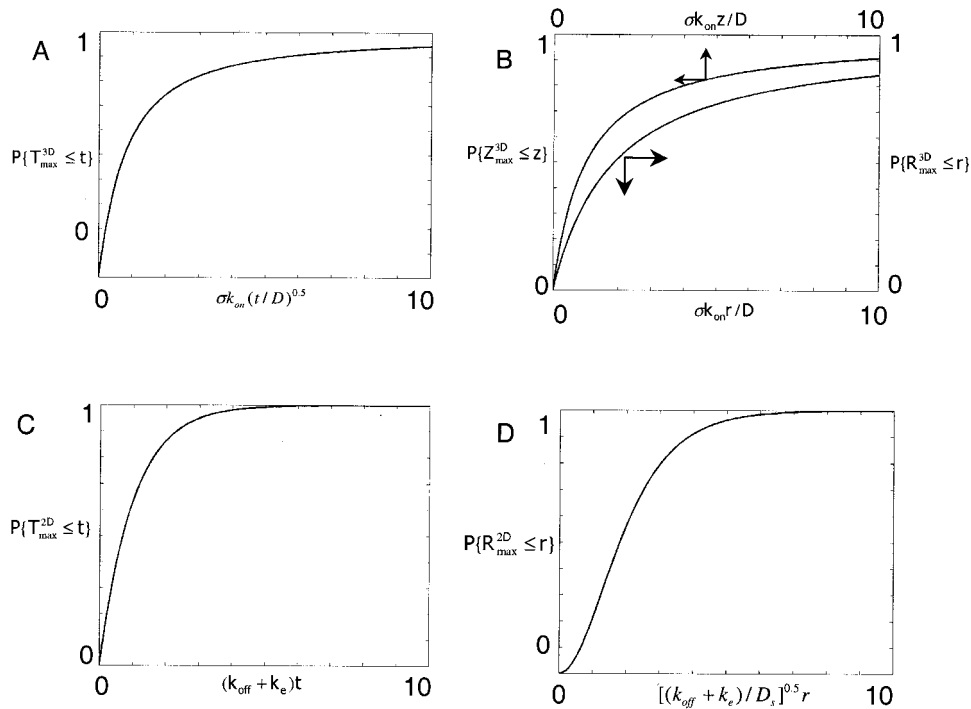


FIGURE 3 Distribution functions characterizing the spatiotemporal extent of the two- and three-dimensional parts of “composite” trajectories. Cumulative distribution functions are plotted as functions of their dimensionless arguments.

drawing a random number, N , from the geometric distribution with parameter δ ; N is the number of returns to the surface. For a fixed N , Z_{\max} is generated by calculating a maximum of N independent random numbers distributed according to $P\{Z_{\max} \leq z\}$, Eq. 1. For a fixed N , \bar{R}_{\max} is generated by adding two terms, which correspond to the sum of N random variables distributed according to $P\{R_{\max}^{3D} \leq r\}$ and $P\{R_{\max}^{2D} \leq r\}$. In the similar generation of T_{\max} , the two terms correspond to the sum of the N random variables distributed according to $P\{T_{\max}^{3D} \leq t\}$ and $P\{T_{\max}^{2D} \leq t\}$.

For each of the random variables Z_{\max} , \bar{R}_{\max} , and T_{\max} , generation of 10^4 realizations took ~ 2 min on a 450 MHz PC. To determine the cumulative distribution functions for Z_{\max} , \bar{R}_{\max} , or T_{\max} , we first generated multiple realizations (10^4) of the corresponding random variable. An accurate discrete approximation of the corresponding distribution function was then assembled through statistical analysis of the resulting database.

EXAMPLE APPLICATION: AUTOCRINE LOOPS IN THE EGFR SYSTEM

In this section, we use our continuum and stochastic models to analyze autocrine loops in the EGFR system. Signaling through EGFR is critical in defining and modulating normal physiological responses, such as cell proliferation, differentiation, and motility (Casci and Freeman, 1999; Davies et al., 1999; Hackel et al., 1999; Kim et al., 1999; Wells, 1999,

2000; Zwick et al., 1999). At the same time, dysregulation of the various parts of the EGFR system has been correlated with several stages of tumorigenesis (Tang et al., 1997; Kim et al., 1999; Wells, 2000; O-Cahroenhat et al., 2000). EGFR belongs to the class of receptor tyrosine kinases (Zwick et al., 1999; Wells, 1999; Moghal and Sternberg, 1999). Bound receptors dimerize, cross-phosphorylate their cytoplasmic tails at several tyrosine residues, forming a signaling complex that provides a scaffold for the components of intracellular signaling cascades (Schlessinger, 2000). Activation of EGFR system is commonly accomplished by locally produced ligands and can be classified as paracrine, autocrine or juxtacrine. It is known that EGFR ligands are produced in the form of membrane-bound precursors that are processed into soluble form by membrane metalloproteases (Massague and Pandiella, 1993). In several cases, it was demonstrated that biological activity of soluble ligands is much greater than that of their membrane-bound precursors. In the EGFR system, the perturbation of the external part of autocrine loops critically affects cell's proliferative and migratory patterns, and the ability of cells to self-assemble in multicellular structures (Wiley et al., 1998; Dong et al., 1999; Tokumaru et al., 2000; Kalmes et al., 2000).

Equilibrium and kinetic parameters for binding and trafficking in growth factor receptor systems, including the ErbB1-4 system to which the EGFR belongs, have been well documented; furthermore, experiments either reporting

diffusivities of growth factors in tissues or allowing their estimation from data have recently started to appear (Dowd et al., 1999; Strigini and Cohen, 2000; Haller and Saltzman, 1998; Entchev et al., 2000). These data can be directly incorporated into our models of autocrine loops.

First, we analyze the steady probability of ligand capture by a single autocrine cell. Fixing the value of rate constants k_{off} , k_c , and k_e —the intrinsic parameters of autocrine loops, we examine the effects of parameters that can be manipulated—the rates of ligand and receptor synthesis (Dong, 1999; Dong et al., 1999; DeWitt et al., 2001). In our model, this amounts to the variations in the Damköhler (Da) and Autocrine (Au) numbers. Using Eq. 14, we plot the lines of constant capture probability, P_{cap} , in the Da – Au plane, Fig. 4.

Consider an autocrine cell equipped with 10^5 receptors and producing one ligand molecule per second (the lower limit of secretion rates reported in DeWitt et al., 2001). At fixed values for the rates of ligand and receptor synthesis, the Au and Da depend on the extracellular ligand diffusivity, D . Reported values D for peptide growth factors range from 10^{-7} cm²/s in free solution to 10^{-11} cm²/s in the extracellular matrix (ECM) (Dowd et al., 1999). Low values of ligand diffusivity arise from the combination of geometric and hydrodynamic effects with the reversible ligand binding to the components of the ECM (Johnson et al., 1996). In our model, changing the extracellular ligand diffusivity with all parameters held constant, shifts the autocrine cell along the line $Da/Au = q/R_T k_{\text{off}}$. We predict that, depending on the value of extracellular ligand diffusivity, our cell can recover from 10 to 65% of endogenous ligand. Hence, our analysis of steady ligand recapture probability indicates that autocrine cells can be very efficient in recapturing the endogenous ligand and, accordingly, that autocrine loops can operate already at a single cell level.

Recent experiments with autocrine systems indicate that ligand release is dynamically regulated through the activity of ligand-releasing proteases (Arribas et al., 1996; Carpenter, 1999; Dent et al., 1999; Dethlefsen et al., 1998; Diaz-Rodriguez et al., 2000; Doedens and Black, 2000; Fan and Derynck, 1999; Gechtman et al., 1999). To examine the dynamics of ligand-receptor binding induced by a step-change increase of the rate of ligand release we use the time-dependent continuum model, Eqs. 12–13. As we see in Fig. 5, steady receptor occupancy can be achieved relatively quickly, within 15–30 min. Note that the reduced model provides a very accurate approximation to the transient computed with the full model, Eqs. 6–9.

We now turn to the analysis of random trajectories followed by autocrine ligands. Consider a confluent monolayer or an epithelial layer of autocrine cells. We start by analyzing the effect of ligand diffusion in the extracellular medium. In Fig. 6 A, the distribution function $P\{Z_{\text{max}} \leq z\}$, which quantifies the probability that the ligand is bound for the first time before diffusing to the height z above the cell surface, is plotted for

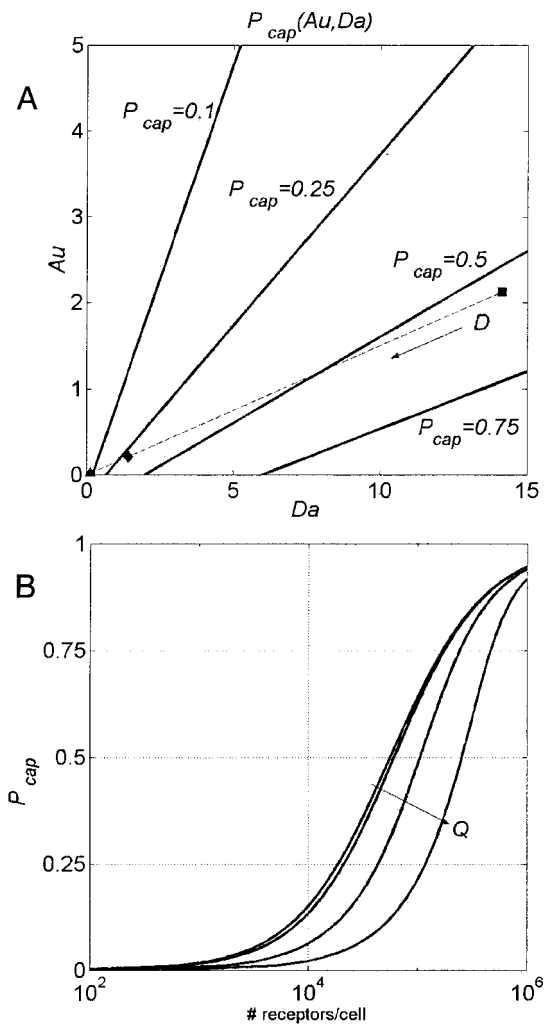


FIGURE 4 Steady-state analysis of the continuum model. (A) Lines of equal probability of capture in the Au – Da plane computed with Eq. 14 for $\gamma = 0.1$ and $\delta = 0.5$. P_{cap} for a single autocrine cell computed as a function of the extracellular ligand diffusivity. Parameters used: $K_d = 10^{-12}$ moles/cm³, $k_{\text{off}} = 1/60 * 0.1$ s⁻¹, $k_{\text{on}} = 1/60 * 10^{11}$ moles⁻¹ cm³s⁻¹, $k_c = 1/60 * 0.01$ s⁻¹, $k_e = 1/60 * 0.1$ s⁻¹, $r_{\text{cell}} = 5 * 10^{-4}$ cm, $Q = 1$ molecule/s/cell, 10^5 receptors/cell; $D = 10^{-9}, 10^{-8}, 10^{-7}$ cm²/s. (B) P_{cap} for a single autocrine cell as a function of the number of receptors/cell computed for several values of ligand release rate. $Q = 1/60 * 1, 100, 1000, 4000$ molecules/cell/s; all other parameters as in (A).

several values of the effective diffusivity D . In these computations, the surface receptor density corresponds to 10^5 receptors uniformly distributed over the surface of a disk-like cell with 10- μm diameter. We see that, at $D = 10^{-9}$ cm²/s, 90% of the ligand molecules are bound before reaching the height of one micron. Autocrine loops become progressively localized as D decreases. Charged ligands strongly interacting with components of ECM, such as HB-EGF, will have even smaller values of effective diffusivities ($D < 10^{-10}$ cm²/s); autocrine loops formed by these ligands are likely to be even more localized. This means that absorbing boundary placed at heights above 1 μm above the layer of autocrine cells will have

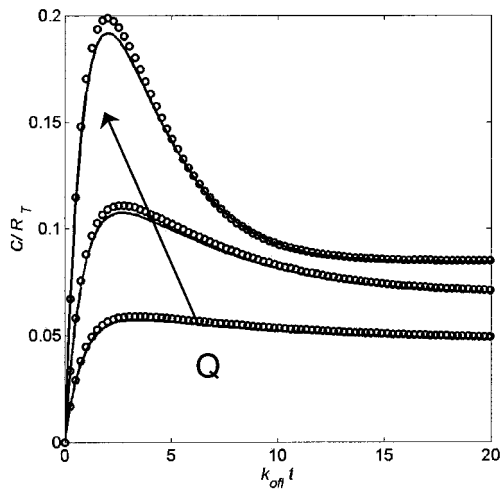


FIGURE 5 Evolution in the number of ligand receptor complexes (scaled by the total number of receptors/cell, $R_T \equiv s/k_c$) in response to a step-change in ligand secretion computed with a continuum model. Time is scaled by the dissociation rate constant of the ligand/receptor complex. In the computation, $k_{off} = 1/60 * 0.1 \text{ s}^{-1}$, $R_T \equiv s/k_c = 10^5$ receptors/cell, Q was changed from 0 to $1/60 * 1000$, $1/60 * 2000$, and $1/60 * 4000$ molecules/cell/s. All other parameters as in Fig. (A). *Solid line*: Full model Eqs. 6–9. *Circles*: Pseudo-steady-state approximation, Eqs. 12–13. The PDE for the spatial distribution of endogenous ligand was discretized using 100 equidistant intervals.

negligible effect on the statistical properties of the trajectories followed by autocrine ligands. Thus, prior to the first binding event, autocrine ligands sample a very small volume.

Our analysis was done for the case when the extracellular ligand diffusivity is space independent. The structural and biochemical complexity of the extracellular matrices is only now starting to be appreciated. The cell surface proteoglycans can reversibly bind peptide growth factors, lowering the value of the effective diffusion coefficient next to the surface. To analyze the effects in the spatial variation of the diffusion coefficient, e.g., lower value of diffusivity next to the surface, consider the case when the diffusivity is a piecewise constant function of the height above layer of autocrine cells. Straightforward modification of the boundary value problem (Eq. A9) for the case with the space-dependent diffusivity leads to the following expression for the cumulative distribution function characterizing the maximal vertical displacement:

$$P\{Z_{\max}^{3D} \leq z\} = \begin{cases} \frac{\sigma k_{on} z / D_1}{1 + \sigma k_{on} z / D_1} & z \leq z_1, \\ \frac{\sigma k_{on} z / D_2 + z_1 / D_1 - z_1 / D_2}{1 + \sigma k_{on} z / D_2 + z_1 / D_1 - z_1 / D_2} & z > z_1. \end{cases} \quad (25)$$

The effect of the nonuniformity in the diffusivity on ligand recapture is presented in Fig. 6 B. Note that 90% capturing efficiency of the homogeneous medium with $D = 10^{-8} \text{ cm}^2/\text{s}$

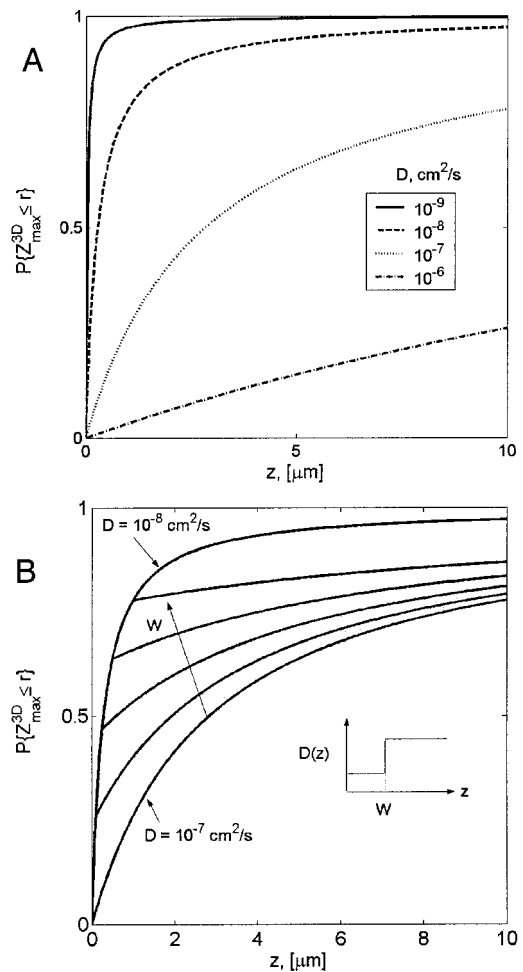


FIGURE 6 Autocrine loops in the model of the EGFR/EGF system: analysis of random trajectories. (A) Effect of the ligand diffusivity in the extracellular medium on the distribution function for the radial component of the three-dimensional segment computed for $k_{on} = 1/60 * 10^{11} \text{ moles}^{-1} \text{ cm}^3 \text{ s}^{-1}$ and 10^5 receptors/cell. (B) Effect of the spatially nonuniform extracellular ligand diffusivity. Diffusivity is a stepwise function of the height above the cell surface,

$$D = \begin{cases} D_1, & z \leq w \\ D_2, & z > w \end{cases}$$

Computation parameters: $D_1 = 10^{-8} \text{ cm}^2/\text{s}$, $D_2 = 10^{-7} \text{ cm}^2/\text{s}$; $w = 0, 0.1 * 10^{-4}, 0.25 * 10^{-4}, 0.5 * 10^{-4},$ and $1 * 10^{-4} \text{ cm}$.

can be realized in the medium where $D = 10^{-7} \text{ cm}^2/\text{s}$ and the surface is surrounded with the low diffusivity layer of one micron. Hence, the parameters that characterize the nonuniformity in the spatial distribution of ligand transport properties can play critical roles in governing the operation of autocrine loops (and other ligand/receptor systems).

We have also calculated the minimal number of surface receptors that ensures that a ligand is bound, for the first time, with high probability (95%) before diffusing to a radial distance equal to the linear dimension of the cell. For this, the inequality $P\{R_{\max}^{3D} \leq r_{\text{cell}}\} \geq 0.95$ has to hold

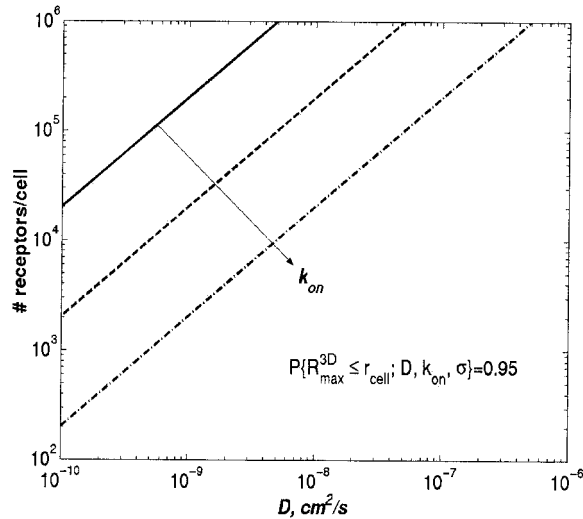


FIGURE 7 Number of surface receptors needed to ensure that ligand is bound for the first time before diffusing to a distance equal to the linear dimension of the cell (5×10^{-4} cm), plotted as a function of ligand diffusivity for several values of k_{on} , $1/60 \times 10^{10}$, $1/60 \times 10^{11}$, and $1/60 \times 10^{12}$ moles $^{-1}$ cm 3 s $^{-1}$. Computations are based on Eq. 22.

($r_{cell} \approx 5 \mu\text{m}$). Using Eq. 22, the calculation of the requisite surface density is done analytically. The requisite number of surface receptors is an increasing function of D , as shown in Fig. 7. The figure also illustrates the sensitivity of the requisite number of surface receptors to the forward binding rate constant. The higher the value of k_{on} , the greater is the spatial localization of autocrine loops. Consequently, fewer receptors are needed to ensure binding within a specified distance, if k_{on} is large.

Multiple binding events preceding the eventual ligand internalization delocalize autocrine loops. This is illustrated in Fig. 8, A and B, which show the functions $P\{Z_{max} \leq z\}$ and $P\{R_{max} \leq r\}$ for several values of the parameter k_{off}/k_e ; the magnitudes for vertical and radial excursions increase with k_{off}/k_e . Recall that the average number of binding events is $N = 1 + k_{off}/k_e$. The rate constants of ligand dissociation and endocytic internalization are approximately equal for the EGFR/EGF pair; hence $N \approx 2$. We have found that, even at $D = 10^{-9}$ cm 2 /s, autocrine loops are quite localized for the parameters and receptor densities characteristic of the EGFR system. Although the value of the surface diffusion coefficient, D_s , has no effect on the vertical extent of autocrine loops, it strongly affects their radial span. In fact, surface diffusion becomes the main source of the radial dispersion when $D > 10^{-8}$ cm 2 /s.

Surface mobility of ligand/receptor complexes in growth factor systems can be impeded by their interaction with cytoskeletal components and by the presence of “corrals” that compartmentalize the cell surface (Saxton, 1994, 1995, 1996, 1997; Saxton and Jacobson, 1997) in our computations we use $D_s = 10^{-11}$ cm 2 /s.

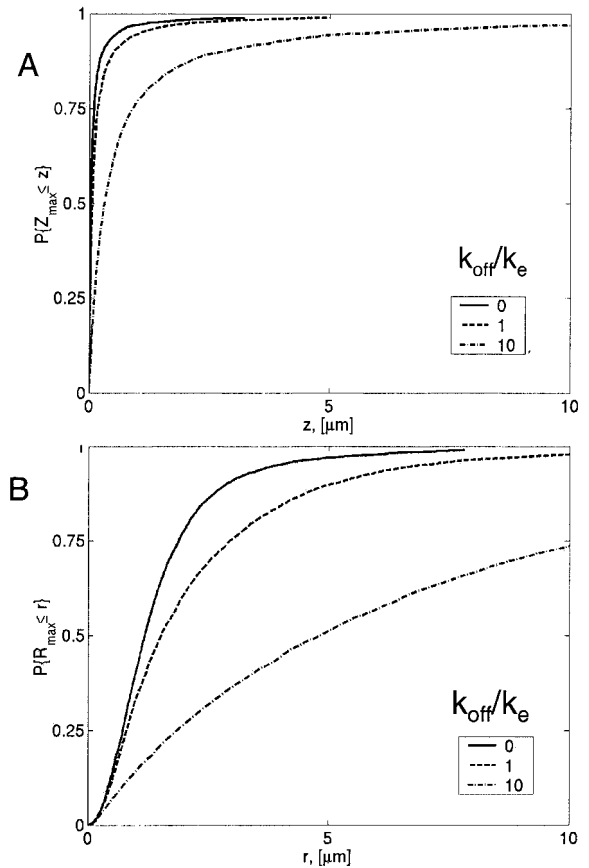


FIGURE 8 Effect of multiple binding events. The number of binding events is given by $N = 1 + k_{off}/k_e$. Radial and vertical distribution functions computed for $D = 10^{-9}$ cm 2 /s, $D_s = 10^{-11}$ cm 2 /s and several values of k_{off}/k_e . The distribution functions were constructed using the Monte Carlo algorithm in Appendix C.

CONCLUSIONS

We have developed mechanistic models of binding and transport in autocrine systems. The continuum model allows the evaluation of the steady and transient ligand recapture probabilities as functions of the ligand diffusivity, kinetic and equilibrium binding constants, and internalization rate constants characterizing the ligand/receptor pair. A stochastic description of the extremal properties of trajectories followed by autocrine ligands provides direct estimates for the spatial range of autocrine loops. Applying our models to study autocrine loops in the EGFR system, we found that the distances over which cells communicate with their environment using secreted endogenous ligands can vary from submicron to tens of microns as a function of such parameters, as receptor density and endocytic rates. Thus, cells have the capability to tune the range of their autocrine loops through the regulation of gene expression levels and choice of ligand family members. These levels of regulation are certainly present in the EGFR system: Cells equipped with the EGFR autocrine loops release several types of the EGFR

ligands, such as heparin-binding EGF, transforming growth factor alpha, and amphiregulin. Concurrently secreted ligands can differ in their binding affinities, levels of their interaction with the extracellular matrix, and binding/trafficking rate constants. Surface receptor densities are regulated by a variety of mechanisms, from relatively fast receptor-mediated endocytosis, to slower changes at the level of gene expression. Rates of EGFR ligand release can be differentially regulated by surface metalloproteases. Such versatility in autocrine regulation is likely to be characteristic of other growth factor and cytokine systems. This indicates that an important fraction of information processing in cell communication can take place even before the intracellular signaling circuitry is engaged.

Both the deterministic and stochastic models are easy to use. The evaluation of the steady capture probability involves solving a single algebraic equation, Eq. 14. The transient binding and transport problem had been converted to a second-order dynamical system that serves as an accurate approximation of the original model, Eqs. 12–13. The distribution functions characterizing the spatiotemporal extrema of the two- and three-dimensional random paths are provided by explicit analytical expressions, Eqs. 20–24. We have to rely on the simulation when computing the distribution functions of composite (a mix of two- and three-dimensional) random paths. These simulations, however, are straightforward to implement and extremely efficient; our Monte Carlo procedure relies on the analytically available distribution functions for the extrema of individual, two- and three-dimensional segments.

We have used our models and algorithms to analyze the operation of autocrine loops in the EGFR system. Based on the continuum model, we conclude that autocrine cells can be very efficient in recapturing endogenous ligand. Hence, autocrine loops can operate already at the level of a single cell. This is consistent with experiments that report that effects of autocrine signaling can be detected in migratory responses of single epithelial cells equipped with the EGFR autocrine loops (Dong et al., 1999). In these experiments interrupting autocrine loops at the stages of ligand release or recapture, using inhibitors of ligand-releasing proteases or receptor-blocking antibodies resulted in significant changes of the speed and persistence of random walks executed by autocrine epithelial cells. Using our stochastic model, we have found that, prior to their capture, autocrine loops sample a very small volume of the extracellular medium. Specifically, in the EGFR system, autocrine ligand is bound for the first time before it has a chance to leave the “pillbox” with the characteristic dimension of 2–3 μm . This estimate is important in light of recent findings in developmental biology, reporting that, in developing tissues, autocrine signaling through the EGF receptor proceeds in the spatially restricted manner. Specifically, in the *Drosophila* oogenesis, secreted ligand Spitz (a homologue of the mammalian TGF α) has been estimated to act on 3–4 cells (Stevens,

1998). Note that, in most of the experimental reports of autocrine systems, the spatial range of autocrine loops is inferred from indirect measurements: e.g., changes of the cell migratory parameters or spatial distribution of the expression of the gene activated by the activated receptor. Our models provide fast access to the estimates of the quantitative characteristics of autocrine loops that cannot be easily or directly measured.

Both the deterministic and stochastic approaches can be easily extended to account for other processes of ligand/receptor systems, such as recycling of internalized ligands and receptors. A combination of ligand diffusion, binding, internalization, and recycling has been recently shown to define the morphogen gradients in the developing tissues (Strigini and Cohen, 2000; Entchev et al., 2000). These quantitative measurements of the spatial distribution of the ligands and its target genes can be used together with our models to extract the kinetic and transport parameters from a system that cannot be easily reconstituted using the cell tissue culture experiments.

Spatially restricted operation of autocrine loops might have important consequences for the dynamics of intracellular cell signaling. Rapidly mounting experimental evidence indicates that proteolytic release of growth factors can be activated by the signal transduction pathways that are stimulated by the corresponding growth factor receptors. In an autocrine cell operating in the regime of efficient ligand recapture, this can establish a positive feedback loop. Indeed, positive feedback has been identified in the EGFR system: the EGFR stimulates the Ras-MAPK pathway, that, through still ill-defined processes, activates ligand-releasing protease, leading to a further increase of receptor occupancy and activation (Dent et al., 1999). Using this positive feedback loop, autocrine cells can fine-tune their responses to exogenous stimuli. Specifically, both the duration and the amplitude of signaling through the Ras-MAPK pathway can be influenced by the autocrine loops. When autocrine loops are closed, i.e., endogenous ligands are recaptured, the dynamics of MAPK induced by a transient exogenous stimulus is large amplitude and persistent; when the autocrine loop is interrupted at the stage of ligand return to the surface, the dynamics of induced MAPK signaling is low-amplitude and transient. The fact that secreted growth factors can bind to the components of the extracellular matrix indicates that the dynamics of intracellular signaling induced in an autocrine cell by exogenous stimuli is sensitive to the composition of cellular microenvironment. Hence, spatially localized autocrine loops emerge as modules for (extracellular) context-dependent signaling. This mechanism of context-dependent cell signaling, efficient ligand recapture + positive feedback involving ligand release, provides a working model for the “cell sonar” hypothesis, according to which autocrine cells use endogenous ligands to probe the composition of their microenvironment (Lauffenburger et al., 1998).

APPENDIX A: RANDOM PATHS LEADING TO THE FIRST CAPTURE

Consider a Brownian particle moving in the half-space above a plane covered by traps, which are distributed with surface density σ . Trapping is characterized by the forward rate constant k_{on} . The cumulative distribution functions of random variables $T_{\text{max}}^{3\text{D}}$, $R_{\text{max}}^{3\text{D}}$, and $Z_{\text{max}}^{3\text{D}}$ depend on parameters σ , k_{on} , and D ,

$$P\{T_{\text{max}}^{3\text{D}} \leq t\} = F_T(t, \sigma, k_{\text{on}}, D), \quad (\text{A1})$$

$$P\{R_{\text{max}}^{3\text{D}} \leq r\} = F_R(r, \sigma, k_{\text{on}}, D), \quad (\text{A2})$$

$$P\{Z_{\text{max}}^{3\text{D}} \leq z\} = F_Z(z, \sigma, k_{\text{on}}, D). \quad (\text{A3})$$

The first step in our derivation of approximate expressions for these distribution functions involves averaging of the heterogeneity of the trapping surface. In this way, the surface is modeled as trapping everywhere, with the surface reaction rate constant k_{eff} . This effective rate constant appears in the boundary condition of a diffusion equation that describes the evolution of the probability density function of particle coordinates. In the simplest approximation, $k_{\text{eff}} = \sigma k_{\text{on}}$. Deriving effective rate constants from the structural parameters of heterogeneous systems, in this case a two-dimensional surface covered by partially absorbing traps, is the subject of active research (Zwanzig and Szabo, 1991; Belyaev et al., 1999; Torquato, 1991).

Let $p(\vec{r}, t|\vec{r}_0, 0)$ denote the probability density function of particle coordinates at time t , given that, initially, the particle was located at $\vec{r}_0 = (x_0, y_0, z_0)$. The evolution of $p(\vec{r}, t|\vec{r}_0, 0)$ is governed by diffusion equation,

$$\frac{\partial p}{\partial t} = D \left[\frac{\partial^2 p}{\partial x^2} + \frac{\partial^2 p}{\partial y^2} + \frac{\partial^2 p}{\partial z^2} \right], \quad (\text{A4})$$

$$p(\vec{r}, t|\vec{r}_0, 0) = \delta(\vec{r} - \vec{r}_0), \quad (\text{A5})$$

$$D \frac{\partial p}{\partial z} \Big|_{z=0} = k_{\text{eff}} p. \quad (\text{A6})$$

The chosen approximation for the effective boundary condition on the trap-covered surface is based on using the low-density limit for k_{eff} and on the steady-state value of the bimolecular reaction rate constant (Zwanzig and Szabo, 1991). Because these assumptions provide a lower bound for k_{eff} (Belyaev et al., 1999), our estimates of the spatial and temporal extent of autocrine loops will be conservative. Hence, autocrine loops will be even more localized than predicted by our analysis.

With heterogeneity in the boundary condition removed, we can derive expressions for the distribution functions characterizing extrema of the Brownian paths leading to the first capture. Approximations for the distribution functions F_Z , F_R , and F_T , obtained using the effective boundary condition, are denoted by G_Z , G_R , and G_T , respectively. The derivation of G_Z , G_R , and G_T follows the standard analysis of splitting probabilities, i.e., the probability of a diffusing particle being absorbed by one of several competing boundaries (Weiss, 1994; Berezhkovskii et al., 1999).

The probability, $P\{Z_{\text{max}}^{3\text{D}} \leq z\}$, that a particle is absorbed before reaching the height z is equivalent to the probability of a particle getting absorbed before reaching a perfectly absorbing plane located at the height z . In complete analogy, $P\{R_{\text{max}}^{3\text{D}} \leq r\}$ is found as the probability that a particle, starting on the partially absorbing plane, is absorbed before reaching the perfectly absorbing surface of a cylinder with radius r . In both cases, we derive the probability of escape from the partially absorbing plane to the perfectly absorbing surface. The splitting probabilities are functions of the starting coordinates, z_0 and r_0 , of a particle. Problems for splitting probabilities lead to Laplace's equation; the boundary condition is unity on the absorbing surface to which the particle is escaping, and partially absorbing on the plane from which the particle starts (Weiss, 1994; Schuss, 1980; Berezhkovskii et al., 1999).

Formally, if the probabilities of escape to the perfectly absorbing surfaces are denoted by $\varepsilon(z_0)$ and $\varepsilon(z_0, r_0)$, respectively, then

$$G_Z(z, k_{\text{eff}}, D) = 1 - \varepsilon(0), \quad (\text{A7})$$

$$G_R(R, k_{\text{eff}}, D) = 1 - \varepsilon(0, 0). \quad (\text{A8})$$

We now specify the boundary value problems for ε . For the Brownian particle starting at $z_0 \in [0, z]$, the probability of escaping to the perfectly absorbing boundary at height z is given by the solution of the boundary value problem,

$$\frac{d^2 \varepsilon}{dz_0^2} = 0, \quad \varepsilon|_{z_0=z} = 1, \quad D \frac{d\varepsilon}{dz_0} \Big|_{z_0=0} = k_{\text{eff}} \varepsilon. \quad (\text{A9})$$

For the Brownian particle, starting inside the infinitely tall cylinder of radius r , the probability of escaping to the perfectly absorbing side is given by

$$\frac{1}{r_0} \frac{\partial}{\partial r_0} r_0 \frac{\partial \varepsilon}{\partial r_0} + \frac{\partial^2 \varepsilon}{\partial z_0^2} = 0, \quad (\text{A10})$$

$$\varepsilon|_{z_0=\infty} = 1, \quad \frac{\partial \varepsilon}{\partial z_0} \Big|_{z_0=0} = k_{\text{eff}} \varepsilon, \quad \frac{\partial \varepsilon}{\partial r_0} \Big|_{r_0=0} = 0, \quad \varepsilon|_{r_0=r} = 1. \quad (\text{A11})$$

Note that, although we are solving for escape probabilities in the domain bounded by the trapping surfaces, we are interested in solutions evaluated only at a single point. We need $\varepsilon(0)$ and $\varepsilon(0, 0)$ for the first and second boundary value problems, respectively. Both problems can be solved analytically. The solutions, expressed in terms of dimensionless variables $\bar{z} = k_{\text{eff}} z / D$ and $\bar{r} = k_{\text{eff}} r / D$ are

$$G_Z(Z, k_{\text{eff}}, D) = G_Z(\bar{z}) = \frac{\bar{z}}{1 + \bar{z}}, \quad (\text{A12})$$

$$\begin{aligned} G_R(R, k_{\text{eff}}, D) &= G_R(\bar{r}) \\ &= \sum_{n=1}^{\infty} \frac{2\bar{r}}{\lambda_n(\bar{r} + \lambda_n) J_1(\lambda_n)} \\ &> \frac{\bar{r}}{1.87 + \bar{r}}, \end{aligned} \quad (\text{A13})$$

where λ_n are zeros of J_0 , Bessel function of the first kind of order zero, and J_1 is the Bessel function of the first kind of order one (Abramowitz and Stegun, 1964). The inequality in Eq. A13 comes from approximation to the infinite series in expression for G_R . Although this series, involving zeros of Bessel functions, can be summed numerically, it is not convenient for use in applications. The last inequality is strict, with the maximum difference between exact G_R and its approximation being less than 2%.

The cumulative distribution $G_T(t, k_{\text{eff}}, D)$ is found as the probability that a Brownian particle, moving on a half-line with a partially absorbing

boundary and starting at that location, has not been absorbed by time t . The transient problem leading to $G_T(t, k_{\text{eff}}, D)$ is

$$G_T(t, k_{\text{eff}}, D) = 1 - \int_0^\infty p(z, t) dz, \quad (\text{A14})$$

$$\frac{\partial p}{\partial t'} = D \frac{\partial^2 p}{\partial z^2}, \quad (\text{A15})$$

$$D \left. \frac{\partial p}{\partial z} \right|_{z=0} = k_{\text{eff}} p, \quad p(z, t' = 0) = \delta(z). \quad (\text{A16})$$

Solution to this problem can be found in the literature (Weiss, 1994),

$$\begin{aligned} G_T(t, k_{\text{eff}}, D) &= 1 - \text{Erfcx}(\bar{t}) \\ &= 1 - e^{\bar{t}^2} \left[1 - \frac{2}{\sqrt{\pi}} \int_0^{\bar{t}} e^{-\eta^2} d\eta \right], \end{aligned} \quad (\text{A17})$$

where $\bar{t} \equiv k_{\text{eff}} \sqrt{t/D}$. Our analytical results are summarized by Eqs. 5–7 in the paper.

APPENDIX B: EXTREMA STATISTICS FOR SURFACE DIFFUSION

Before being removed from the surface, bound ligands diffuse with an effective diffusion coefficient D_s ; this increases the radial extent of auto-crine loops. In this appendix, we formulate and solve a boundary value problem describing the distribution of the maximal radial distances to which a particle can diffuse before it is removed from the surface. The probability, $P\{R_{\text{max}}^{2D} \leq r\}$, that the maximal distance, R_{max}^{2D} , traveled on the surface is less than r , can be found as the probability that a particle is removed before reaching the perfectly absorbing boundary at radius r .

Consider a two-dimensional Brownian particle starting inside a circular domain with a perfectly absorbing boundary. A particle can disappear on the boundary of the domain, or it can leave the surface due to a first-order process with a total rate constant $\kappa \equiv k_{\text{off}} + k_e$. The probability, $\varphi(r_0, t)$, that a particle, starting at r_0 , “reacts” in the time interval $(t, t + dt)$ is proportional to the product two probabilities,

$$\varphi(r_0, t) = \kappa e^{-\kappa t} S(t|r_0). \quad (\text{B1})$$

The first term, $\kappa e^{-\kappa t}$, is the probability that a particle, not yet reacted at time t , reacts between t and $t + dt$. The second term, $S(t|r_0)$, is the so-called “survival probability,” i.e., the probability that the particle, in the absence of reaction, is still inside the circle at time t . It is defined as

$$S(t|r_0) = \int_0^r 2\pi p(\rho, t|r_0, 0) \rho d\rho, \quad (\text{B2})$$

where $p(\rho, t|r_0, 0)$ is the probability density function of the radial coordinate of a Brownian particle diffusing inside a circle of radius r with absorbing boundary. The probability that a particle starting at r_0 reacts before reaching the boundary is denoted by $\Phi(r_0)$. It is found by integrating the expression for $\varphi(r_0, t)$ over all times,

$$\Phi(r_0) \equiv \int_0^\infty \varphi(r_0, t) dt. \quad (\text{B3})$$

Following these definitions, the probability that a particle is removed from the surface before its radial coordinate reaches r is found as

$$P\{R_{\text{max}}^{2D} \leq r\} = \int_0^\infty \varphi(0, t) dt = \Phi(0). \quad (\text{B4})$$

Hence our goal is to obtain the dependence of Φ on the radius of the domain.

The derivation relies on the properties of survival probability $S(t|r_0)$. A well-known result in the theory of Brownian motion (Berezkhovskii et al., 1999) states that survival probability satisfies the adjoint equation,

$$\frac{\partial S}{\partial t} = \frac{D_s}{r_0} \frac{\partial}{\partial r_0} \left(\frac{\partial S}{\partial r_0} \right) \equiv D_s \nabla_{r_0}^2 S, \quad (\text{B5})$$

where $\nabla_{r_0}^2$ is the radial part of Laplace operator in cylindrical coordinates. Applying that operator to both sides of Eq. B3, multiplying by D_s and using Eqs. B3 and B5 gives

$$\begin{aligned} D_s \nabla_{r_0}^2 \Phi &= D_s \nabla_{r_0}^2 \int_0^\infty \kappa e^{-\kappa t} S(t|r_0) dt \\ &= \int_0^\infty \kappa e^{-\kappa t} \frac{\partial S(t|r_0)}{\partial t} dt. \end{aligned} \quad (\text{B6})$$

Integrating the last expression by parts, we obtain

$$D_s \nabla_{r_0}^2 \Phi = -\kappa + \kappa \Phi. \quad (\text{B7})$$

The boundary conditions are posed by requiring that Φ is finite everywhere in the domain and zero on the boundary; clearly, for a particle starting on the boundary, the chance of reacting is zero. The solution is found in terms of the modified Bessel function of the first kind of order zero (Abramowitz and Stegun, 1964):

$$\Phi(r_0) = 1 - \frac{I_0(r_0 \sqrt{\kappa/D_s})}{I_0(r \sqrt{\kappa/D_s})}. \quad (\text{B8})$$

For the probability that the particle, released at the origin, is dissociated or internalized before its radial coordinate increases to r , we obtain

$$\begin{aligned} P\{R_{\text{max}}^{2D} \leq r\} &= \varphi(r_0 = 0) \\ &= 1 - I_0(r \sqrt{(k_e + k_{\text{off}})/D_s})^{-1}. \end{aligned} \quad (\text{B9})$$

This work was partially funded by NIH Grant HD28528 and DARPA Grant MDA972-00-1-0030 to D.A.L. and by NIH Postdoctoral Fellowship F32 GM20847 to S.Y.S. S.Y.S. is indebted to Drs. A.M. Berezkhovskii, A. Szabo, and G. H. Weiss (NIH) for providing a draft of their book on diffusion-limited reactions.

REFERENCES

- Abramowitz, M., and I. A. Stegun. 1964. Handbook of Mathematical Tables with Formulas, Graphs, and Mathematical Tables. U.S. GPO, Washington, DC.
- Agmon, N., and A. L. Edelstein. 1997. Collective binding properties of receptor arrays. *Biophys. J.* 72:1582–1594.
- Arribas, J., L. Coodly, P. Vollmer, T. K. Kishimoto, S. RoseJohn, and J. Massague. 1996. Diverse cell surface protein ectodomains are shed by a

- system sensitive to metalloprotease inhibitors. *J. Biol. Chem.* 271: 11376–11382.
- Belyaev, A. G., G. A. Chechkin, and R. R. Gadyl'shin. 1999. Effective membrane permeability: estimates and low concentration asymptotics. *SIAM J. Appl. Math.* 60:84–108.
- Berezkhovskii, A., A. Szabo, and G. H. Weiss. 1999. Notes on diffusion-influenced reactions. (Manuscript)
- Berg, H. C., and E. M. Purcell. 1977. Physics of chemoreception. *Biophys. J.* 20:193–219.
- Carpenter, G. 1999. Employment of the epidermal growth factor receptor in growth factor-independent signaling pathways. *J. Cell Biol.* 146:697–702.
- Casci, T., and M. Freeman. 1999. Control of EGF receptor signalling: lessons from fruitflies. *Can. Metast. Rev.* 18:181–201.
- Dagpunar, J. 1988. Principles of Random Variable Generation. Clarendon Press, Oxford, U.K.
- Davies, D. E., R. Polosa, S. M. Pudicombe, A. Richter, and S. T. Holgate. 1999. The epidermal growth factor receptor and its ligand family: their potential role in repair and remodelling in asthma. *Allergy.* 54:771–783.
- Deen, W. M. 1998. Analysis of Transport Phenomena. Oxford University Press, New York.
- Dent, P., D. Reardon, J. Park, G. Bowers, C. Logsdon, K. Valerie, and R. Schmidt-Ullrich. 1999. Radiation-induced release of transforming growth factor alpha activates the epidermal growth factor receptor and mitogen-activated protein kinase pathway in carcinoma cells, leading to increased proliferation and protection from radiation-induced cell death. *Mol. Biol. Cell.* 10:2493–2506.
- Dethlefsen, S. M., G. Raab, M. A. Moses, R. M. Adam, M. Klagsbrun, and M. R. Freeman. 1998. Extracellular calcium influx stimulates metalloproteinase cleavage and secretion of heparin-binding EGF-like growth factor independently of protein kinase C. *J. Cell Biol.* 69:143–153.
- DeWitt, A., J. Y. Dong, H. S. Wiley, and D. A. Lauffenburger. 2001. Quantitative analysis of the EGF receptor autocrine system reveals cryptic regulation of cell response by ligand capture. *J. Cell Sci.* 114: 2301.
- Diaz-Rodriguez, F., A. Esparis-Ogando, J. C. Montero, L. Yuste, and A. Pandiella. 2000. Stimulation of cleavage of membrane proteins by calmodulin inhibitors. *Biochemical J.* 346:359–367.
- Doedens, J. R., and R. A. Black. 2000. Stimulation-induced down-regulation of tumor necrosis factor-alpha converting enzyme. *J. Biol. Chem.* 275:14598–14607.
- Dong, J. Y., L. K. Opreko, P. J. Dempsey, D. A. Lauffenburger, R. J. Coffey, and H. S. Wiley. 1999. Metalloprotease-mediated ligand release regulates autocrine signaling through the epidermal growth factor receptor. *Proc. Natl. Acad. Sci. U.S.A.* 96:6235–6240.
- Dowd, C. J., C. L. Cooney, and M. A. Nugent. 1999. Heparan sulfate mediates BFGF transport through basement membrane by diffusion with rapid reversible binding. *J. Biol. Chem.* 274:5236–5244.
- Entchev, E., A. Schwabedissen, and M. Gonzalez-Gaitan. 2000. Gradient formation of the TGF-beta homolog Dpp. *Cell.* 103:981–991.
- Fan, H. Z., and R. Derynck. 1999. Ectodomain shedding of TGF-alpha and other transmembrane proteins is induced by receptor tyrosine kinase activation and MAP kinase signaling cascades. *EMBO J.* 18:6962–6972.
- Forsten, K. E., and D. A. Lauffenburger. 1994a. Probability of ligand capture by cell-surface receptors: implication for ligand secretion measurements. *J. Comp. Biol.* 1:15–25.
- Forsten, K. E., and D. A. Lauffenburger. 1994b. The role of low-affinity interleukin-2 receptors in autocrine ligand-binding—alternative mechanisms for enhanced binding effect. *Mol. Immunol.* 31:739–751.
- Freeman, M. 2000. Feedback control of intercellular signalling in development. *Nature.* 408:6810, 313–319.
- Gechtman, Z., J. L. Alonso, G. Raab, D. E. Ingber, and M. Klagsbrun. 1999. The shedding of membrane-anchored heparin-binding epidermal-like growth factor is regulated by the Raf/mitogen-activated protein kinase cascade and by cell adhesion and spreading. *J. Biol. Chem.* 274:28828–28835.
- Goldring, S. R., and M. B. Goldring. 1996. Cytokines and skeletal physiology. *Clin. Orthop.* 323:13–23.
- Goldstein, B., and M. Dembo. 1995. Approximating the effects of diffusion on reversible reactions at the cell surface: ligand-receptor kinetics. *Biophys. J.* 68:1222–1230.
- Hackel, P. O., E. Zwick, N. Prenzel, and A. Ullrich. 1999. Epidermal growth factor receptors: critical mediators of multiple receptor pathways. *Curr. Opin. Cell Biol.* 11:184–189.
- Haller, M., and W. Saltzman. 1998. Localized delivery of proteins in the brain: can transport be customized? *Pharm. Res.* 15:377–385.
- Johnson, E. M., D. A. Berk, R. K. Jain, and W. M. Deen. 1996. Hindered diffusion in agarose gels: Test of effective medium model. *Biophys. J.* 70:1017–1023.
- Kalmes, A., B. Vesti, G. Daum, J. Abraham, and A. Clowes. 2000. Heparin blockade of thrombin-induced smooth muscle cell migration involves inhibition of epidermal growth factor (EGF) receptor transactivation by heparin-binding EGF-like growth factor. *Circulation Res.* 87:92–98.
- Kim, H. G., J. Kassis, J. C. Souto, T. Turner, and A. Wells. 1999. EGF receptor signaling in prostate morphogenesis and tumorigenesis. *Histol. Histopathol.* 14:1175–1182.
- Kuwada, S. K., K. A. Lund, X. F. Li, P. Cliften, K. Amsler, L. K. Opreko, and H. S. Wiley. 1998. Differential signaling and regulation of apical vs. basolateral EGFR in polarized epithelial cells. *Am. J. Physiol. Cell Physiol.* 44:C1419–C1428.
- Lagerholm, B. C., and N. L. Thompson. 1998. Theory for ligand rebinding at cell membrane surfaces. *Biophys. J.* 74:1215–1228.
- Lauffenburger, D. A., K. E. Forsten, B. Will, and H. S. Wiley. 1995. Molecular/cell engineering approach to autocrine ligand control of cell function. *Ann. Biomed. Eng.* 23:208–215.
- Lauffenburger, D. A., G. T. Oehrtman, L. Walker, and H. S. Wiley. 1998. Real-time quantitative measurement of autocrine ligand binding indicates that autocrine loops are spatially localized. *Proc. Natl. Acad. Sci. U.S.A.* 95:15368–15373.
- Massague, J., and A. Pandiella. 1993. Membrane-anchored growth-factors. *Ann. Rev. Biochem.* 62:515–541.
- Moghal, M., and P. W. Sternberg. 1999. Multiple positive and negative regulators of signaling by the EGF-receptor. *Curr. Opin. Cell Biol.* 11:190–196.
- O-Cahroenhat, P., P. Rhys-Evans, and S. Eccles. 2000. Expression and regulation of c-ERBB ligands in human head and neck squamous carcinoma cells. *Int. J. Cancer.* 88:759–765.
- Oehrtman, G. T., H. S. Wiley, and D. A. Lauffenburger. 1998. Escape of autocrine ligands into extracellular medium: experimental test of theoretical model predictions. *Biotech. Bioeng.* 57:571–582.
- Ross, S. 1972. Introduction to Probability Models. Academic Press, New York.
- Saxton, M. J. 1994. Anomalous diffusion due to obstacles—a Monte-Carlo study. *Biophys. J.* 66:394–401.
- Saxton, M. J. 1995. Single-particle tracking—effects of corrals. *Biophys. J.* 69:389–398.
- Saxton, M. J. 1996. Anomalous diffusion due to binding: A Monte Carlo study. *Biophys. J.* 70:1250–1262.
- Saxton, M. J. 1997. Single-particle tracking: the distribution of diffusion coefficients. *Biophys. J.* 72:1744–1753.
- Saxton, M. J., and K. Jacobson. 1997. Single-particle tracking: applications to membrane dynamics. *Ann. Rev. Biophys. Biomol. Struct.* 26:373–399.
- Schlessinger, J. 2000. Cell signaling by receptor tyrosine kinases. *Cell.* 103:211–225.
- Shi, W., H. Z. Fan, L. Shum, and R. Derynck. 2000. The tetraspanin CD9 associates with transmembrane TCF-alpha and regulates TGF-alpha-induced EGF receptor activation and cell proliferation. *J. Cell Biol.* 148:591–601.
- Shoup, D., and A. Szabo. 1982. Role of diffusion in ligand-binding to macromolecules and cell-bound receptors. *Biophys. J.* 40:33–39.
- Sporn, M., and A. Roberts. 1992. Autocrine secretion—10 years later. *Ann. Intern. Med.* 117:408–414.
- Sporn, M., and G. Todaro. 1980. Autocrine secretion and malignant transformation of cells. *N. Engl. J. Med.* 303:878–880.

- Starbuck, C., H. S. Wiley, and D. A. Lauffenburger. 1990. Epidermal growth-factor binding and trafficking dynamics in fibroblasts—relationship to cell-proliferation. *Chem. Eng. Sci.* 45:2367–2373.
- Stevens, L. 1998. Twin peaks: spitz and argos star in patterning of the *Drosophila* embryo. *Cell*. 95:291–294.
- Strigini, M., and S. Cohen. 2000. Wingless gradient formation in the *Drosophila* wing. *Curr. Biol.* 10:293–300.
- Tang, P., P. A. Steck, and W. K. Yung. 1997. The autocrine loop of TGF- α /EGFR and brain tumors. *J. Neurooncol.* 35:303–314.
- Tokumaru, S., S. Higashiyama, T. Endo, T. Nakagawa, J. Miyagawa, K. Yamamori, Y. Hanakawa, H. Ohmoto, K. Yoshino, Y. Shirakata, Y. Matsuzawa, K. Hashimoto, and N. Taniguchi. 2000. Ectodomain shedding of epidermal growth factor receptor ligands is required for keratinocyte migration in cutaneous wound healing. *J. Cell Biol.* 151: 209–220.
- Torquato, S. 1991. Diffusion and reaction among traps—some theoretical and simulation results. *J. Statist. Physics.* 65:1173–1206.
- Wang, D., S. Y. Gou, and D. Axelrod. 1992. Reaction-rate enhancement by surface-diffusion of adsorbates. *Biophys. Chem.* 43:117–137.
- Weiss, G. H. 1994. Aspects and Applications of the Random Walk. North-Holland, Amsterdam.
- Wells, A. 1999. EGF receptor. *Int. J. Biochem. Cell Biol.* 31:637–643.
- Wells, A. 2000. Tumor invasion: role of growth factor-induced cell motility. *Adv. Cancer Res.* 78:31–101.
- Werb, Z., and Y. Yan. 1998. A cellular striptease act. *Science*. 282: 1279–1280.
- Wiley, H. S., M. F. Woolf, L. K. Opreko, P. M. Burke, B. Will, J. R. Morgan, and D. A. Lauffenburger. 1998. Removal of the membrane-anchoring domain of epidermal growth factor leads to intracrine signaling and disruption of mammary epithelial cell organization. *J. Cell Biol.* 143:1317–1328.
- Zwanzig, R., and A. Szabo. 1991. Time-dependent rate of diffusion-influenced ligand-binding to receptors on cell-surfaces. *Biophys. J.* 60: 671–678.
- Zwick, E., P. Hackel, N. Prenzel, and A. Ullrich. 1999. The EGF receptor as central transducer of heterologous signalling systems. *Trends Pharmacol. Sci.* 20:408–412.